Catalysis Today 432 (2024) 114599

Contents lists available at ScienceDirect

Catalysis Today

journal homepage: www.elsevier.com/locate/cattod

The comparison of photocatalytic reduction of CO_2 on ZnO photocatalysts at slightly acidic and alkaline pH towards the formation of valuable products

Ewelina Kusiak-Nejman *, Katarzyna Ćmielewska, Ewa Ekiert, Agnieszka Wanag, Joanna Kapica-Kozar, Iwona Pełech, Urszula Narkiewicz, Antoni W. Morawski

Department of Inorganic Chemical Technology and Environment Engineering, Faculty of Chemical Technology and Engineering, West Pomeranian University of Technology in Szczecin, Pułaskiego 10, Szczecin 70-322, Poland

ARTICLE INFO

Keywords:
Heterogeneous CO_2 photoreduction
Homogeneous CO_2 photoreduction
ZnO photocatalyst
Zinc oxide

ABSTRACT

The photocatalytic reduction of CO_2 to carbon monoxide, methane and hydrogen (as a valuable byproduct) in the suspension or solution of various Zn-based forms in an alkaline environment and water, respectively, was investigated. These are the first results showing homogeneous CO_2 photoreduction in the presence of Zn-based photocatalysts in an inorganic environment.

The ZnO photocatalysts were suspended in the alkaline environment, while in water, they completely dissolved during at least 6 hours of carbonation, forming a transparent solution. The small crystallite size also determines a high zinc solubility in an aqueous solution (97.7 % for 14 nm, 92.2 % for 25 nm, and 68.5 % for crystallites larger than 100 nm). This homogeneous solution showed a slightly lower photoactivity than the heterogeneous suspension because of a lower concentration of crucial bicarbonate HCO_3^- ions. In both cases, the selectivity gives the order H_2>CO>CH_4. It was suggested that the photoactive centres in the dissolved agglomerates are the –Zn–O–Zn– hydrous bridges, which can use bicarbonate (HCO_3^-) ions as a transporter of CO_2. In addition, the H^+ ions generated during the ZnO dissolving in water can first participate in the CO_2 photoreduction towards CO and CH_4 and, afterwards, involve forming small quantities of hydrogen.

1. Introduction

Carbon dioxide utilisation is becoming one of the most significant challenges of our time. One of the many directions studied is using photocatalysis to reduce CO_2 and obtain valuable products such as carbon monoxide, methane, methanol and other hydrocarbons with selectivity depending on the photocatalyst's type, composition and physicochemical properties. The most commonly used photocatalysts based on TiO_2 and ZnO are modified and treated in various ways. Photocatalysts in the form of n-type semiconductors like ZnO with a wide band gap of 3.37 eV are recommended as very effective, non-toxic, and stable in the reactions to water purification from organic compounds [1,2]. Patial et al. [3] presented a comprehensive discussion on the current development and new directions in the engineering of ZnO-based photocatalysts concerning the reduction of carbon dioxide to valuable chemicals (i.e. CO, CH_4, HCOOH, and CH_3OH), including the mechanisms of CO_2 reduction reactions to the products mentioned above. Adegoke and co-workers [4] emphasized that controlling the shape and size of preferred ZnO materials and optimal adjustment of their chemical and physical properties is crucial for their optimal reactivity and selectivity in the photocatalytic conversion of CO_2. The authors established that utilizing a hydrothermal method for sample preparation led to obtaining different ZnO structures (shape, size, and orientation), significantly affecting the reduction of CO_2 to valuable products. Additionally, it is possible to prepare ZnO semiconductors characterised by a higher population of (001) Zn-polar faces with the enhanced ability to enhance the photocatalytic activity of CO_2 photoreduction.

Many papers also discuss the effect of zinc oxide modification with various compounds on the efficiency of the CO_2 photoreduction process [5–10]. The ZnO quantum dots loaded onto KNb_3O_8 nanosheets [5], constituting form a heterojunction with KNb_3O_8 nanosheets, demonstrated superior photocatalytic activity with 1539.77 μmol/g/h of methanol yield. Furthermore, the mechanism of photocatalytic

* Corresponding author.
E-mail address: ekusiak@zut.edu.pl (E. Kusiak-Nejman).

https://doi.org/10.1016/j.cattod.2024.114599
Received 27 November 2023; Received in revised form 7 February 2024; Accepted 19 February 2024
Available online 21 February 2024

reduction of CO_2 is photogenerated electrons and holes to be consumed for producing methanol and acetone (from simultaneous oxidation of isopropanol) separately. An effective approach to obtaining efficient photocatalysts based on semiconducting metal oxides for CO_2 reduction with remarkable abilities to absorb lights, separating charge carriers and CO_2 presented by Li et al. [6]. A hollow structured p-n heterojunction catalyst, polydopamine (PDA)-ZnO/Co_3O_4, was synthesised by pyrolysing bimetallic ZnCo-ZIFs, followed by modification with PDA. The processes were performed in a mixed solvent of dimethylformamide DMF with water under UV-Vis light irradiation without any photosensitiser and additional sacrificial reagents. Photocatalyst PDA15/ZnO/Co_3O_4 showed a carbon monoxide production rate of 537.5 μmol/g/h with a CO selectivity of 97.7 %. The combination of CdS and ZnO, forming a CdS/ZnO heterojunction photocatalyst, leads to higher activity for reducing CO_2 to fuels than that of CdS under visible light irradiation [7]. In this heterojunction, the CdS/ZnO structure separated electrons from ZnO by migrating electrons and capturing them in CdS. In the mixture of 15 % CO_2 and 85 % argon and 10 mL of water over the CdS/ZnO photocatalyst, 35.2 μmol/g/h of CO and 5.9 μmol/g/h of CH_4 under the visible lamp and 0.4 MPa pressure during 4 hours of irradiation were measured. Zhang et al. [8] proposed a photocatalytic reduction mechanism in the presence of ZnO/ZnSe composites containing heterojunction type II that were prepared by a simple solvothermal method for photocatalytic CO_2 reduction. It was concluded that the photocatalytic activity of the sample containing 3 wt % of ZnO/ZnSe was significantly higher than that of bare ZnO, and ZnSe 1581.82 μmol/g_{cat}/h of methanol was produced with the use of mentioned material. The highest rate of methanol is attributed to the heterojunction structure in the composite for effectively transferring carriers and simultaneously inhibiting the recombination of electrons and holes.

An outline of recent achievements in the classification of metal oxide defects based on the dimensions of a host crystal lattice was presented by Raizada et al. [9]. The authors described a surface modification of metal oxides through 0D (point), 1D (line), 2D (planar), and 3D (volume) defects with their subsequent mechanism and impact on photocatalytic performance. Additionally, it was pointed out that the electronic configuration created by defects modulates the electron-hole pair dynamics, stability, and active radicals production for various oxides, including ZnO. Alhebshi et al. [10], on the other hand, widely discussed extensively advancement in semiconductors and their characteristics toward the photoreduction of CO_2, including ZnO, focused on their limitation and possibilities of overcoming them by doping and co-doping to reduce band gap or cocatalyst by noble metals and nonmetals. They analysed semiconductor advancements concerning quantum dots, heterojunction, and sacrificial reagents.

Interestingly, Guo et al. [11] proposed ZnO_2-promoted ZnO synthesised via H_2O_2 treatment. The authors revealed that an excess of ZnO_2 increased the surface area and enhanced oxygen vacancies, significantly improving the adsorption capacity of molecular CO_2. So, the obtained ZnO_2-promoted ZnO photocatalyst showed a 21 times enhanced ability for CO_2 reduction to methane and methanol in comparison to pristine ZnO.

There are also known porous ZnO nanoplates with vacancy defects synthesised by annealing ZnS(en)0.5 precursor in the air at a different temperature [12]. The defect amount in ZnO changes with the annealing temperature (600–700 °C), resulting in other photocatalytic activity for CO_2 reduction. It was found that the creation of oxygen defects affects the selectivity of the reduction of CO_2 and leads to producing only carbon monoxide. After 4 hours of photoreaction, 3.8 μmol/g of carbon monoxide was analysed for ZnO obtained at 600 °C. This material also had the highest content of V_O defects. Additionally, ZnO was found to be unstable during operation because $Zn_5(OH)_6(CO_3)_3$ phases appeared on the surface, which are transient during CO_2 photoreduction, and its defects are promoters of the acid-base Lewis interaction. The discussion on the presence of a $Zn_5(OH)_6(CO_3)_3$ form was further developed in the work by Xin et al. [13]. The authors found that $Zn_5(OH)_6(CO_3)_2$ (also used in our study as a reference material) strongly adsorbed on the ZnO nanosheet surface, which is believed to be the active intermediate species formed due to Lewis acid-base interactions and finally facilitated the photocatalytic reduction of CO_2 to CO and CH_4. The results show that the porous ZnO nanosheets, with more defect sites, that is, zinc and oxygen vacancies, exhibit a much higher activity for the photoreduction of CO_2 with H_2O when compared to ZnO nanoparticles and nanorods. With the use of prepared ZnO with oxygen vacancies, 1122.69 μmol/g_{cat}/h of H_2, 406.77 μmol/g_{cat}/h of CO, and 20.16 μmol/g_{cat}/h of CH_4 were produced at 200 °C.

From the point of view of our work, not only the presence of the $Zn_5(OH)_6(CO_3)_3$ form will determine the efficiency of the photoreduction of CO_2 into valuable products, but Since the reaction slurry was saturated with CO_2, an equilibrium CO_2 between the gas phase dissolved in water as carbonate and bicarbonate ion should also be considered. Pang et al. [14] experimentally found an influence of this phenomenon on the photoactivity of CO_2 reduction to CO. The HCO_3^- ions were beneficial for improving photoactivity and selectivity to CO by increasing carbon-related species on the surface of the photocatalyst's surface, suppressing the backward reaction of CO_2 conversion. Using a solution of $NaHCO_3$ with a pH of 8–10, the photoactivity conversion of CO_2 to CO with bubbling of argon was significantly higher than only water solution with a pH of 4–5.

In this study, we hypothesise that such a bicarbonate or carbonate complex with zinc is the keyway to the photocatalytic reduction of dioxide with the participation of ZnO. The second hypothesis is that both a heterogeneous and homogeneous system based on zinc oxide, adjusted by changes in pH solution, can be used for the photocatalytic reduction of CO_2. For the experiments illustrating the above-presented hypotheses, we selected ZnO with two extremely low particle sizes (<26 nm) and high (<5 μm), as well as the material in the form of basic zinc carbonate $(ZnCO_3)_2{\cdot}[Zn(OH)_2]_3$ as reference material that plays a crucial role in CO_2 reduction as suggested elsewhere [12–14]. The suspensions of the above photocatalysts were tested at a slightly acidic pH in water and at alkaline pH in NaOH solution. In both cases, saturation with CO_2 was used before the photocatalytic CO_2 reduction reaction.

Based on current knowledge, it can be stated that this is the first article that discusses the reduction of CO_2 by using ZnO dissolved in water (homogeneous photocatalysis without any organic metal complex). In addition, the homogeneous photocatalytic activity was compared to a heterogeneous one (tested in alkaline conditions) utilising the same photocatalysts.

2. Experimental

2.1. Materials

Three various zinc-containing materials were used in photocatalytic CO_2 reduction processes. They differed in structure and particle size. The first was ZnO with low particle size, up to 26 nm. It was produced by the Institute of High Pressure Physics (Polish Academy of Science, Poland) using methods of microwave solvothermal synthesis as given in the literature [15]. The second one was ZnO, with a particle size of up to 5 μm (Sigma-Aldrich, USA). The last one was reagent-grade basic zinc carbonate used as a reference material $(ZnCO_3)_2{\cdot}[Zn(OH)_2]_3$ (Firma Chempur, Poland).

2.2. Materials characterisation

The surface functional groups of tested samples were determined by the FT-IR 4200 spectrometer (JASCO International Co. Ltd., Japan) supplied with DiffuseIR accessory (PIKE Technologies, USA). The FT–IR spectra were examined in the 4000–400 cm^{-1} range.

The phase composition of tested samples was performed on the Empyrean PANalytical diffractometer (Malvern PANanalytical Ltd., United Kingdom) utilising Cu Kα radiation (λ Cu Kα= 0.1540 nm,

measurement range of 10–70°). The HighScore+ softwere and International Center for Diffraction Data PDF4+ 2018 database were used for the phase identification (00-036-1451 PDF4+ card for ZnO, 01-072-1100 PDF4+ card for $Zn_5(CO_3)_2(OH)_6$ and 00-003-0787 PDF4+ card for $Zn_4(CO_3)(OH)_6{\cdot}H_2O$). The average crystallite size was calculated from Scherrer's equation.

The specific surface area (S_{BET}) was determined in the relative pressure range of 0.05–0.3 and calculated based on Brunauer-Emmett-Teller (BET) equation utilising N_2 adsorption-desorption isotherms performed on a QUADRASORB evo™ Gas Sorption automatic system (Quantachrome Instruments GmbH & Co. KG, USA) at 77 K (−196 °C). Before the experiment, samples were outgassed at 100 °C under a vacuum of $1{\cdot}10^{-5}$ mbar for 12 h using a MasterPrep multi-zone flow/vacuum degasser (Quantachrome Instruments GmbH & Co. KG, USA) to remove adsorbed species that could intervene in the adsorption processes.

The surface morphology of the samples was investigated with SEM Hitachi SU 8020 scanning electron microscope (Hitachi Ltd., Japan). The images were taken at an accelerating voltage of 5 kV and a magnification of 50k and 200k.

ImageJ public domain software was used to analyse ZnO particles from SEM images statistically. Initially, it was necessary to set up the scale, i.e. the number of pixels at a given distance, at a magnification of 200 000x-200 nm. The surface area was determined by manually drawing an appropriate figure representing the shape of the particle for ZnO <26 nm- circle, ZnO <5 μm- polygon, and for $(ZnCO_3)_2{\cdot}[Zn(OH)_2]_3$- ellipse.

The slight difference in crystallite/particle size and specific surface area determined by experimental methods (X-ray diffraction and low-temperature N_2 adsorption-desorption, respectively) and that obtained by modelling with ImageJ software is, i.e. due to the introduction of an assumed form factor for the modelling method. However, it should be noted that, regardless of the method of measurement/modelling, the results obtained show a high level of agreement.

2.3. Photocatalytic performance

The experiments were conducted in two different environments for each sample, using a 0.2 M solution of NaOH or distilled water. The reactor scheme used in experiments with a working capacity of about 766 cm^3 (Heraeus Noblelight GmbH, Germany) was presented in our previous paper [16]. It was also equipped with a quartz cooler supplied with water, where a medium-pressure mercury lamp TQ 150 Z3 (Heraeus Noblelight GmbH, Germany) was placed. The lamp's power was 150 W and had a wide range of UV-Vis radiation (mostly UV-A and UV-C).

200 mg of the tested powder was placed in the reactor. Then, 500 cm^3 of distilled water or 0.2 M aqueous sodium hydroxide solution was added. The pH was equal to 6.9–7.2 and 11.5 for water with dissolved samples and ZnO and basic zinc carbonate suspended in 0.2 M NaOH solution, respectively. The system was rinsed with pure CO_2 (Messer Polska Sp. z o.o., Poland) for 16 hours. It caused a decrease of pH to 5.6–5.8 for an aqueous environment containing dissolved zinc-based compounds and 8.0 for an alkaline environment. For comparison, pure redistilled water used in the experiments had a pH of 5.8, and after 16 hours of CO_2 saturation, the pH decreased to pH 4.17.

Finally, it was closed, and the lamp was turned on. During the process, the gas phase was stirred using the pump with a flow rate equal to 1.6 dm^3/h, and the liquid phase was also continuously mixed with a magnetic stirrer at 400–600 rpm. The system was placed in the thermostatic chamber to ensure a stable process temperature of 20 °C and cut off any external light sources. The processes were carried out for 6 h, and the gas samples for analysis were collected every 1 h.

The gas phase composition was analysed with a Master GC gas chromatograph (DANI Instruments S.p.A., Italy) equipped with a 4 m Shincarbon ST 100/120 micropacked column. The detectors used were TCD and FID with the methanizer. The carrier gas was argon. The gas pressure on the column was 6 bars. The volume of the tested gas sample was 1 cm^3. The content of individual components in the gas phase in subsequent measurements was calculated based on the calibration curve.

After the process, the zinc content in the liquid phase was determined by the ICP-OES technique using the Avio™ 500 spectrometer (PerkinElmer Inc., USA). A certified *Trace*CERT® Ultra zinc standard for ICP (NIST- and BAM-CRM traceable, Sigma-Aldrich, Switzerland) with an initial concentration of 1000 mg/dm^3 ± 2 mg/dm^3 was used to prepare a calibration curve.

3. Results and discussion

In all three samples' FT-IR/DR spectrum (Fig. 1), a broad peak ranging from 2900 to 3700 cm^{-1} is attributed to the characteristic –OH stretching vibration chemisorbed on synthesised ZnO nanoparticles' surface [17,18]. Though the FT-IR/DR spectrum of all tested samples shows similar peak positions for the –OH band, the intensity of this peak differs and is related to the particle size of the sample. The intensity increases with the decrease in ZnO particle size [15]. The –OH groups are also represented by stretching vibration modes of isolated hydroxyl groups, C–O stretch in hydroxyl groups and –OH bending vibration peaks located around 3695, 1089 and 894 cm^{-1}, respectively [15,18]. Some characteristic peaks for ZnO are observed for ZnO <5 μm and ZnO <26 nm samples. Thus, the low intensive bands between 2854 and 2926 cm^{-1} are assigned to the C–H stretching vibration of alkane groups from organic compounds applied to the synthesis [19]. Additionally, C═O and C–H vibration bands related to partially transformed aldehyde or ketone groups from the zinc source acetate ions and the glycol functional group coatings are observed at 1416 and 1644 cm^{-1} [20]. A significant vibration band located in the region from 300 to 680 cm^{-1} is assigned to the characteristic stretching mode of the ZnO bond [21]. The two intensive peaks at 1412 and 1564 cm^{-1} observed for $(ZnCO_3)_2{\cdot}[Zn(OH)_2]_3$ sample are ascribed to the asymmetric ν_3 CO_3^{2-} stretching mode [22,23], while ν_4 CO_3^{2-} and ν_2 CO_3^{2-} are located at 749 and 851 cm^{-1}, respectively [24]. The peaks characteristic of the ZnO bond are observed, similar to ZnO <5 μm and ZnO <26 nm samples, between 300 and 680 cm^{-1}.

It is clear from Fig. 2 that the samples labelled as Zn <26 nm and ZnO <5 μm consist of only hexagonal zincite (00–036–1451 PDF4+ card), whereas the occurrence of two forms was established for basic zinc carbonate: $Zn_5(CO_3)_2(OH)_6$ (01–072–1100 PDF4+ card) and $Zn_4(CO_3)(OH)_6{\cdot}H_2O$ (00–003–0787 PDF4+ card).

SEM imaging of ZnO <26 nm samples (Fig. 3a-c) showed that zinc oxide exists in oval particles, often spheres, that create more oversized agglomerates, marked in Fig. 3c with a dashed line. Using ImagingJ software, the cross-section area of particles seen in Fig. 3b was measured, and assuming that the particles have a shape similar to a sphere, their equivalent diameter was determined. A histogram shown in Fig. 3d was plotted on this basis. Determined particle size distribution (PSD) can be described with Gaussian distribution, where the mean value (μ) of equivalent diameter was 24 nm (very close to average crystallite size determined with XRD method listed in Table 1) and standard deviation (σ) was 3.65 nm. According to these values, it can be stated that 95.5 % of particles have equivalent diameters in the range of 16.7–31.3 nm and 99.7 % in the range of 13.05–34.95 nm. Based on the PSD for ZnO <26 nm sample, the model surface area was calculated to be as high as 45 m^2/g, while the specific surface area determined with the S_{BET} method is 29 m^2/g (see Table 1). These values are comparable, and the difference between them is probably due to the agglomeration process. If 35 % of the particle surface were blocked by sticking with other particles, then the model and specific surface areas became the same.

The zinc oxide sample described as ZnO <5 μm in SEM images shows a much smaller size, where the biggest seen in Fig. 3e-g does not exceed

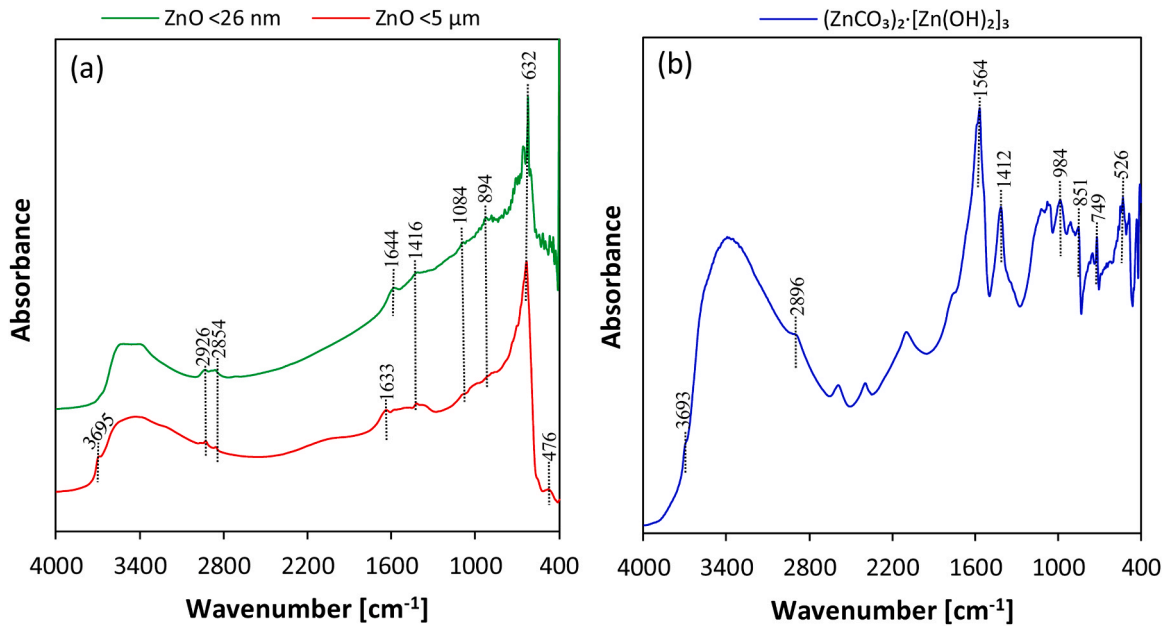

Fig. 1. FTIR/DRS spectra of (a) ZnO <26 nm and ZnO <5 μm and (b) $(ZnCO_3)_2{\cdot}[Zn(OH)_2]_3$.

1 μm, while the smallest one is 25 nm (Table 1). Observed objects have the shape of prisms with different shapes, bases and heights. Using ImageJ software, the cross-section area of over 120 objects seen in Fig. 3g was estimated, and a histogram was plotted (Fig. 3h).

$Zn(CO_3)_2{\bullet}[Zn(OH)_2]_3$ has plates with different diameters and very similar heights close to 14 nm (see Fig. 3i–k). They stick together to form various structures, porous sponges if they touch each other perpendicular, or very tight and concise when plates are lying on themselves parallel. The cross-section area of particles was estimated using the same software. Next, assuming the shape of the plates was a flattened ellipsoid with a smaller diameter to be constant, 14 nm and varying larger diameter, the distribution of equivalent diameter was determined, and then Gaussian distribution was also fitted (Fig. 3l). The mean equivalent diameter, D_2, is 43 nm with standard deviation (σ) equalled 10.5 nm, so 95.5 % of particles have an equivalent diameter from 22 to 64 nm, and 99.7 % in the range 11.5–74.5 nm. The model surface area calculated based on PSD for $Zn(CO_3)_2{\bullet}[Zn(OH)_2]_3$ sample was over 71 m^2/g, while the specific surface area was 40 m^2/g (see Table 1). To equal these two values, 44 % of the particle surface must be in touch with others, like in a parallel plate structure.

After 4 h of CO_2 saturation, it was observed that the $(ZnCO_3)_2{\cdot}[Zn(OH)_2]_3$ suspension in the water has changed to a colourless and transparent aqueous solution without any suspended particles causing turbidity. Also, ZnO <26 nm and ZnO <5 μm materials behaved similarly. Carbonation was carried out for 16 h overnight to ensure the complete dissolution of samples. In the case of the same samples placed in an alkaline solution and similarly saturated with carbon dioxide, no turbidity changes were observed before saturation and after 16 h of CO_2 saturation. Therefore, in all cases, the aqueous phase after the photocatalytic activity measurement processes was analysed for the content of zinc ions. The results of these analyses are presented in Table 2.

From the results presented in Table 2, it can be concluded that all tested samples of photocatalysts, regardless of the particle size, were stable in the alkaline (NaOH) solution after 16 h of carbon dioxide saturation and for the next 6 h of photocatalytic activity measurements. On the other hand, all samples of photocatalysts tested in the water saturated with carbon dioxide practically dissolved (see Fig. 4). It was proved with the zinc content in the filtered solution (Table 2). The determined degree of dissolution was from 68.5 % to 97.7 %. Still, it should be noted that the measurements of zinc content by ICP-OES took several h, and the solution was re-suspended due to the slow desaturation of CO_2 from the samples during the transfer, which changed the carbonate balance in the solution. It can be assumed that all zinc was transferred to the solution and reached 100 %. Interestingly, it was noted that the total dissolved zinc content depends on the size of the crystallites - the smaller the crystallites, the higher the zinc solubility.

The photocatalytic performance of the tested materials in CO_2 reduction to hydrogen, carbon monoxide, and methane was visualised in Fig. 4 and Table 3. Based on the results, it can be seen that material ZnO <26 nm was characterised by the highest photoactivity, both in aqueous and alkaline environments. The amounts of obtained products were 44.78 $\mu mol/g_{photocat.}/dm^3$ of hydrogen, 14.93 $\mu mol/g_{photocat.}/dm^3$ of carbon monoxide, and 1.04 $\mu mol/g_{photocat.}/dm^3$ of methane for the process in an aqueous environment. In contrast, for the test in an alkaline environment product, amounts were 63.92 $\mu mol/g_{photocat.}/dm^3$ of hydrogen, 18.70 $\mu mol/g_{photocat.}/dm^3$ of carbon monoxide, and 4.04 $\mu mol/g_{photocat.}/dm^3$ of methane.

On the contrary, the other two materials showed lower activity, especially in hydrogen production, in which the decrease in the amount was significant (3.20–13.77 $\mu mol/g_{photocat.}/dm^3$). The amount of produced carbon monoxide was decreased only to a lesser extent (9.68–12.83 $\mu mol/g_{photocat.}/dm^3$). The quantity of methane was the lowest in all tests, which can be explained by the fact that it takes 8 electrons to form a methane molecule. Therefore, in this case, the reduction of CO_2 to carbon monoxide was more privileged since it is a 2-electron reaction. The variable hydrogen production rate was probably because it is an intermediate product of carbon dioxide reduction and was continuously consumed in other reactions. It is worth mentioning that all tested materials were active even in an aqueous environment despite being entirely dissolved in water saturated with CO_2. This proves the possibility of carrying out homogeneous photocatalytic processes using the discussed zinc compounds. Another observation can be seen from the results provided. The photocatalytic activities for hydrogen, carbon monoxide, and methane are generally higher in an alkaline aqueous medium compared to pure and neutral water for the same photocatalyst due to a higher concentration of crucial bicarbonate ions in an alkaline environment and lower concentration of this HCO_3^- ions in near neutral pH in water saturated with CO_2.

The use of $(ZnCO_3)_2{\cdot}[Zn(OH)_2]_3$ as the photocatalyst was motivated by the conclusions put forward by Li et al. [12], Xin et al. [13], and Pang

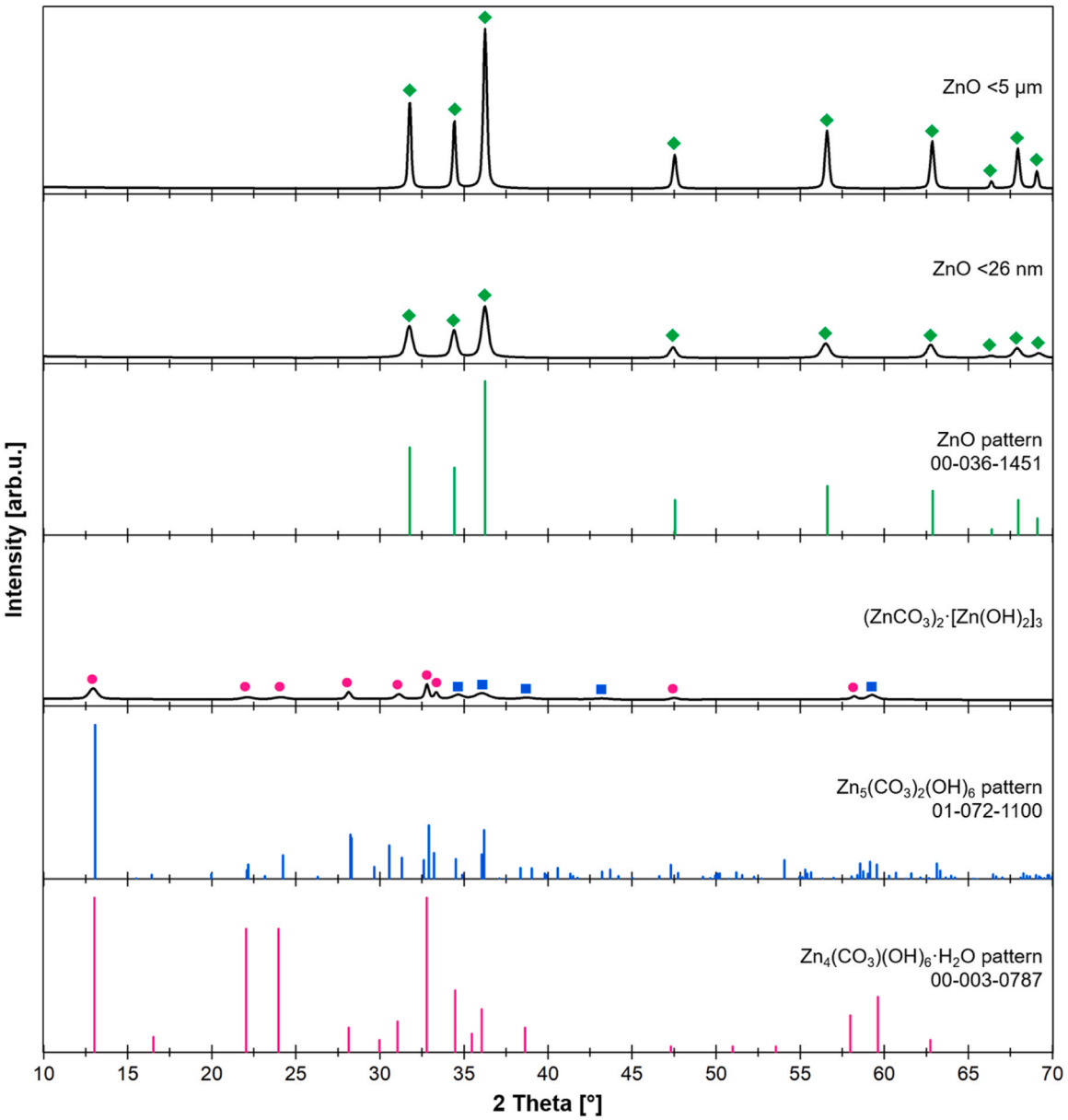

Fig. 2. XRD patterns of ZnO <26 nm, ZnO <5 μm and $(ZnCO_3)_2{\cdot}[Zn(OH)_2]_3$ with the corresponding PDF4+ standard patterns.

et al. [14]. They claimed that the active phase on the surface of various ZnO photocatalysts was exactly $(ZnCO_3)_2{\cdot}[Zn(OH)_2]_3$. This phase results from complex reactions of carbon dioxide with photoactive zinc oxide, which will depend on the carbonate-bicarbonate balance of CO_2 in the aqueous solution [25]. Dissolution of a small part of free carbon dioxide in water leads to the formation of carbonic acid, presented as reaction (1), which is in equilibrium with carbonate and bicarbonate according to the following dissociation reactions (2) and (3) [26]:

$$2CO_2 + H_2O \rightleftharpoons CO_{2(aq)} + H_2CO_3 \quad (1)$$

$$H_2CO_3 \rightleftharpoons HCO_3^- + H^+ \quad (2)$$

$$HCO_3^- \rightleftharpoons CO_3^{2-} + H^+ \quad (3)$$

Based on carbonate speciation as a function of pH, it is known that free CO_2 dissolved in water also forms small portions of chemically unstable carbonic acid, as presented in reaction (1). The highest amounts of H_2CO_3 are found in an acidic pH. Increasing the pH to 4.5 shifts the equilibrium towards bicarbonate formation (reaction (2)) with the dominant fraction of HCO_3^- in the pH regime below 9 [27]. The carbonate fraction, presented in reaction (3), becomes minor at pH 8.5 and dominant above the pH of 11. Saruhashi [26] detailedly analysed the pH-dependent changes in relative speciation of carbon dioxide (CO_2), bicarbonate (HCO_3^-), and carbonate (CO_2^{3-}) in water, i.e. at pH=5.0 and a temperature of 20 °C, 96.2 % carbonic acid, 3.8 % bicarbonate ions, and no carbonate ions were confirmed. At pH=6.0, 71.5 % of carbonic acid, 28.5 % of bicarbonate ions and no carbonate ions were found, and at pH=7.0, only 20 % of carbonic acid, 80 % of bicarbonate ions and no carbonate ions. At basic pH=10.0, no carbonic acid, 70.6 % of bicarbonate ions and 29.94 % of carbonate ions were detected [26].

Due to the above equilibria, in pure water during carbon dioxide saturation of ZnO suspension, regardless of the size of ZnO particles, we have to deal with the following dissolution reactions (4) and (5) of solid particles [28]:

- dominating reaction:

$$ZnO_{(s)} + H_2CO_3 \rightleftharpoons ZnCO_3 + H_2O \quad (4)$$

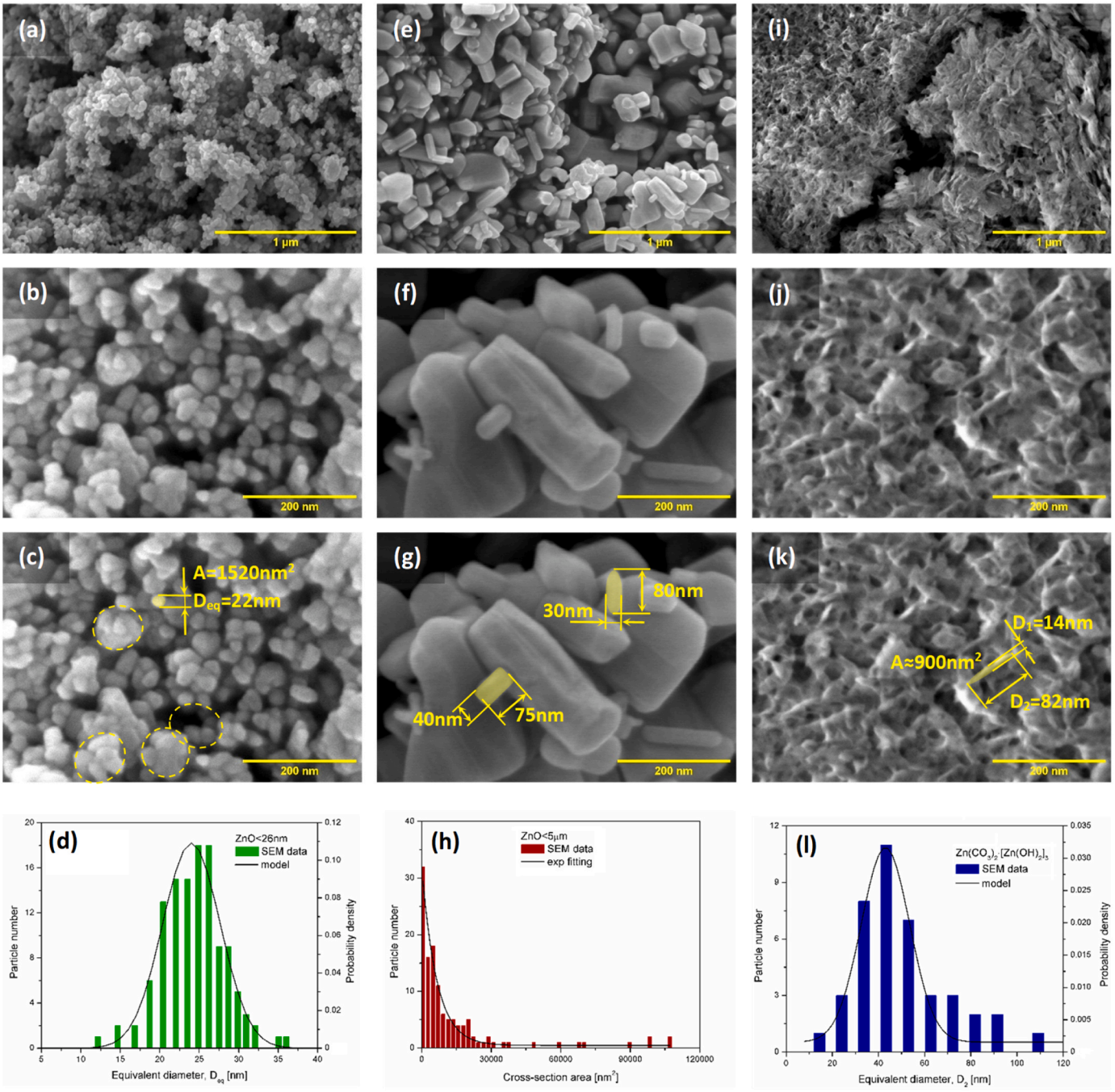

Fig. 3. SEM pictures and histograms presenting particle size distribution of the tested materials: (a–d) ZnO <26 nm, (e–h) ZnO <5 μm, and (i-l) $(ZnCO_3)_2{\cdot}[Zn(OH)_2]_3$ made under various magnifications.

Table 1
The physicochemical properties of ZnO-based photocatalysts.

Sample code	Mean crystallite size [nm] *	Equivalent diameter [nm] **	Specific surface area S_{BET} [m^2/g] ***	Model surface area S_{mod} [m^2/g] **
ZnO <26 nm	25	24	29	45
ZnO <5 μm	>100	25–1000	8	-
$(ZnCO_3)_2{\cdot}[Zn(OH)_2]_3$	14	43	40	71

* X-ray diffraction analysis.
** Modelling analysis using ImageJ public domain software.
*** Low-temperature N_2 adsorption-desorption.

- and side reaction:

$$ZnO_{(s)} + 2CO_2 + H_2O \rightleftharpoons Zn(HCO_3)_{2(aq)} \quad (5)$$

The above equilibrium limitation with dominating reaction (4), reducing abilities of samples to CO_2 reduction reaction to valuable chemicals because only bicarbonate ions HCO_3^- from reaction (5) is useful in this purpose, as concluded by other authors [15,16].

During the saturation of ZnO suspension in sodium hydroxide solution, ZnO particles are stable because the following reactions (6) and (7) occur:

Table 2
The contents of the zinc in the liquid phase were introduced in the form of solid photocatalysts for all materials tested in the aqueous (H_2O) and alkaline (NaOH) solution.

Sample code	Amount of zinc introduced into the reactor [mg]	Amount of zinc analysed in the liquid phase [mg]	Total dissolved zinc [%]
ZnO <26 nm_H_2O	161.4	148.9	92.2
ZnO <26 nm_NaOH	161.4	*BLQ**	0.0
ZnO <5 μm_H_2O	161.5	110.7	68.5
ZnO <5 μm_NaOH	161.5	1.3	0.8
$(ZnCO_3)_2{\cdot}[Zn(OH)_2]_3$_$H_2O$	161.1	157.4	97.7
$(ZnCO_3)_2{\cdot}[Zn(OH)_2]_3$_NaOH	160.9	0.1	0.1

*Beneath Limit of Quantification.

- dominating reaction, which stabilizes the ZnO particles in suspension because carbon dioxide is involved in reactions with sodium ions:

$$ZnO_{(s)} + CO_2 + NaOH + H_2O \rightleftharpoons NaHCO_3 + ZnO_{(s)} + H_2O \quad (6)$$

- side reaction:

Table 3
Contents of products in the gas phase after 6 h of the photocatalytic process.

Sample code	The content in the gas phase after 6 h of the process [μmol/$g_{photocat.}$/dm^3]		
	H_2	CO	CH_4
ZnO <26 nm_H_2O	44.78	14.93	1.04
ZnO <26 nm_NaOH	63.92	18.70	4.04
ZnO <5 μm_H_2O	3.20	10.37	0.74
ZnO <5 μm_NaOH	9.49	12.83	1.05
$(ZnCO_3)_2{\cdot}[Zn(OH)_2]_3$_$H_2O$	10.08	9.68	0.77
$(ZnCO_3)_2{\cdot}[Zn(OH)_2]_3$_NaOH	13.77	11.03	0.52

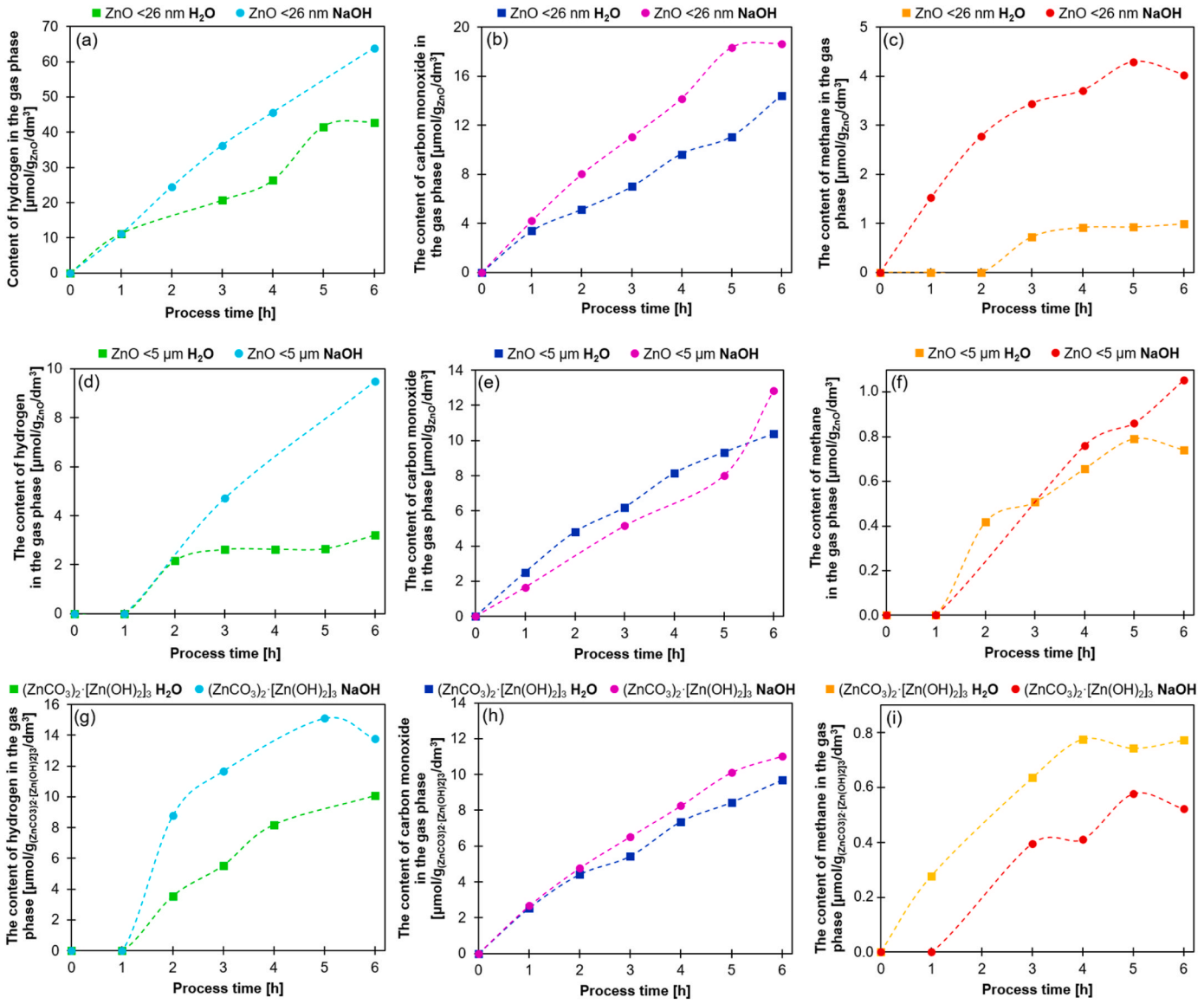

Fig. 4. The content of: (a, d, g) H_2, (b, e, h) CO, and (c, f, i) CH_4 in the gas phase for the sample ZnO <26 nm, ZnO <5 μm and $(ZnCO_3)_2{\cdot}[Zn(OH)_2]_3$, respectively, tested in an aqueous (H_2O) and alkaline (0.2 M NaOH) environment.

$$ZnO_{(s)} + CO_2 + 2NaOH + H_2O \rightleftharpoons Na_2CO_3 + Zn(OH)_2 + H_2O \quad (7)$$

Also, according to the following equilibrium reaction, the ZnO slurry is stable because CO_2 is continuously involved in the reaction (8):

$$2NaHCO_3 \rightleftharpoons Na_2CO_3 + CO_2 + H_2O \quad (8)$$

Both of them, $NaHCO_3$ and Na_2CO_3, are highly soluble in water.

In the above cases of carbonate equilibrium states in an alkaline environment, the presence of small amounts of zinc carbonate ($ZnCO_3$) and zinc hydroxide ($Zn(OH)_2$) cannot be ruled out, which forms a complex compound mentioned as an active phase on the ZnO surface, i.e. basic zinc carbonate $(ZnCO_3)_2{\cdot}[Zn(OH)_2]_3$, which is stable in an alkaline environment, but soluble in neutral and acidic water, i.e. saturated with CO_2. Based on XRD measurements of ZnO photocatalysts, Xin et al. [13] proposed the following reaction (9) to form this phase on ZnO particles at 150–250 °C with water vapour and CO_2:

$$5ZnO + 2CO_2 + 3H_2O \rightleftharpoons Zn_5(OH)_6(CO_3)_2 \quad (9)$$

where: $Zn_5(OH)_6(CO_3)_2$ is $(ZnCO_3)_2{\cdot}[Zn(OH)_2]_3$ in our work.

In summarizing, under the experiment conditions (at slightly acidic pH), after the dissolution of ZnO as well as the possibly formed $(ZnCO_3)_2{\cdot}[Zn(OH)_2]_3$ phase, Zn^{2+} ions dominate [13], co-existing with other characteristic ions (CO_3^{2-}, OH^-, HCO_3^-). While in the alkaline medium in the suspension of ZnO and $(ZnCO_3)_2{\cdot}[Zn(OH)_2]_3$, we are dealing with ZnO mainly, as well as $ZnCO_3$ and $Zn(OH)_2$ particles. These compounds in an alkaline solution can be occluded with water and OH^- groups, e.g. forming $Zn(OH)_4^{2-}$ or surface hydroxyl groups like $(Zn–O)_n–OH$ [27]. The wurtzite ZnO phase stability vs water pH was studied by Yamabi and Imai [29]. At a low pH value, it is expected that $Zn(OH)_2$ dissolves as $Zn(OH)_{2(aq)}$ and Zn^{2+} or dissolved $ZnOH^+$ forms, especially at lower zinc concentrations. They confirmed the presence of $Zn(OH)_4^{2-}$ ions in higher pH.

Reactions (11)–(15), shown below, explain the formation of various hydrated forms of zinc (present as a homogeneous phase) as a result of its dissolution in water following the CO_2 saturation of the suspension:

$$ZnO_{(s)} + H_2O \rightleftharpoons Zn(OH)^+_{(aq)} + OH^- \quad (11)$$

$$Zn(OH)^+_{(aq)} + H_2O \rightleftharpoons Zn(OH)_{2(aq)} + H^+ \quad (12)$$

$$Zn(HCO_3)_{2(aq)} + H_2O \rightleftharpoons Zn^{2+}_{(aq)} + 3OH^- + H^+ + 2CO_2 \quad (13)$$

$$Zn^{2+}_{(aq)} + 2H_2O \rightleftharpoons Zn(OH)_{2(aq)} + 2H^+ \quad (14)$$

$$Zn(OH)_{2(aq)} + 2H_2O \rightleftharpoons Zn(OH)^{2-}_{4(aq)} + 2H^+ \quad (15)$$

At pH> 9, hydroxyl ions from an alkaline solution can react further to produce dissolved zinc hydroxide or hydrated zinc ions again (reactions (16) and (17)):

$$ZnOH^+ + OH^- \rightleftharpoons Zn(OH)_{2(aq)} \quad (16)$$

$$Zn(OH)_2 + 2OH^- \rightleftharpoons Zn(OH)^{2-}_{4(aq)} \quad (17)$$

The above molecules of hydrated zinc hydroxides can form local dissolved networks in which the –Zn–O–Zn– junction is the most essential and photoactive part of the aggregate containing the hydroxyl groups. For example, two molecules of $Zn(OH)_2$ can be transformed as given in a general dehydration reaction (18) [29]:

$$Zn(OH)_n^{2-n} + Zn(OH)_n^{2-n} \rightleftharpoons Zn_2O(OH)_{2n-2}^{4-2n} + H_2O \quad (18)$$

where n=2 or 4.

Hydrogen cations formed in reactions (11)–(15), in addition to H^+ ions from photocatalytic water decomposition, participate in the CO_2 photoreduction towards carbon monoxide and methane according to reactions (19) and (20) [30]:

$$CO_2 + 2H^+ + 2e^- \rightarrow CO + H_2O \quad (19)$$

$$CO_2 + 8H^+ + 8e^- \rightarrow CH_4 + 2H_2O \quad (20)$$

An excess hydrogen ion formed in the reactions (11)–(15) can react with e^- from the conduction band, generated during photoexcitation of ZnO photocatalyst or the –Zn–O–Zn– junction, producing hydrogen as presented in reaction (21):

$$2H^+ + 2e^- \rightarrow H_2 \quad (21)$$

4. Conclusions

The photocatalytic reduction of CO_2 to hydrogen, carbon monoxide, and methane in the suspension or solution of two ZnO forms (ZnO <26 nm and ZnO <5 μm) and $(ZnCO_3)_2{\cdot}[Zn(OH)_2]_3$, used as a reference material, in both an alkaline environment by NaOH and in neutral water was investigated. Because of carbonate-bicarbonate equilibrium, the ZnO samples and reference material were stable in the alkaline environment. The crystallite size was correlated with the high zinc solubility in an aqueous solution (97.7 % for 14 nm, 92.2 % for 25 nm, contrary to 68.5 % for crystallites larger than 100 nm).

The ZnO with an average size of <26 nm was the best with activity. The amount obtained products for ZnO <26 nm were 63.92 μmol/$g_{photocat.}$/dm^3 of H_2, 18.70 μmol/$g_{photocat.}$/dm^3 of CO, and 4.04 μmol/$g_{photocat.}$/dm^3 of CH_4 for the test in an alkaline environment. In an ordinary water environment, all tested samples of zinc-containing compounds are completely dissolved within minutes. 6 h of carbonation of water to form a transparent solution of Zn^{2+} ions coordinated by OH^-, CO_3^{2-}, and HCO_3^-. The solution showed photoactivity with a slightly lower value than the heterogeneous one. Also, the ZnO <26 nm for the process in an aqueous environment was the highest photoactivity because production was 44.78 μmol/$g_{photocat.}$/dm^3 of hydrogen, 14.93 μmol/$g_{photocat.}$/dm^3 of carbon monoxide, and 1.04 μmol/$g_{photocat.}$/dm^3 of methane.

For both cases, selectivity creates the order $H_2 > CO > CH_4$. It has been proposed that the photoactive center in dissolved agglomerates $Zn_2O(OH)_{2n-2}^{4-2n}$ is a hydrous bridge –Zn–O–Zn– that can utilise bicarbonate HCO_3^- ions as a transporter of CO_2. In addition, the H^+ ions generated during the ZnO dissolving in water can first participate in the CO_2 photoreduction towards CO and CH_4 and, secondly, involve forming small quantities of hydrogen as a valuable byproduct.

CRediT authorship contribution statement

Antoni W. Morawski: Writing – review & editing, Writing – original draft, Supervision, Methodology, Investigation, Conceptualization. **Urszula Narkiewicz:** Writing – review & editing, Supervision, Investigation, Funding acquisition, Conceptualization. **Ewelina Kusiak-Nejman:** Writing – review & editing, Writing – original draft, Investigation, Conceptualization. **Agnieszka Wanag:** Writing – review & editing, Writing – original draft, Investigation, Formal analysis. **Katarzyna Ćmielewska:** Writing – review & editing, Writing – original draft, Methodology, Formal analysis, Conceptualization. **Ewa Ekiert:** Writing – original draft, Investigation, Formal analysis, Data curation. **Joanna Kapica-Kozar:** Writing – original draft, Investigation, Formal analysis. **Iwona Pełech:** Supervision.

Data availability

Data will be made available on request.

Acknowledgements/Funding

The research leading to these results has received funding from the Norway Grants 2014–2021 via the National Centre for Research and Development, Poland, under the grant number NOR/POLNORCCS/

PhotoRed/0007/2019-00.

Declaration of Competing Interest

The authors declare the following financial interests/personal relationships which may be considered as potential competing interests: Urszula Narkiewicz reports financial support was provided by National Centre for Research and Development. Antoni W. Morawski has patent Sposób otrzymywania wodoru pending to P.438028. If there are other authors, they declare that they have no known competing financial interests or personal relationships that could have appeared to influence the work reported in this paper.

References

[1] U.K.H.M. Nadzim, N.H.H. Hairom, M.A.H. Hamdan, M.K. Ahmad, A.A. Jalil, et al., J. Alloy. Compd. 913 (2022) 165145, https://doi.org/10.1016/j.jallcom.2022.165145.

[2] P. Kajitvichyanukul, V.H. Nguyen, T. Boonupara, L.A. Phan Thi, A. Watcharenwong, et al., Environ. Res. 212 (2022) 113336, https://doi.org/10.1016/j.envres.2022.113336.

[3] S. Patial, R. Kumar, P. Raizada, P. Singh, Q. Van Le, et al., Environ. Res. 197 (2021) 111134, https://doi.org/10.1016/j.envres.2021.111134.

[4] K.A. Adegoke, M. Iqbal, H. Louis, S.U. Jan, A. Mateen, et al., Pak. J. Anal. Environ. Chem. 19 (2018) 1–27, https://doi.org/10.21743/pjaec/2018.06.01.

[5] X. Shao, W. Xin, X. Yin, Beilstein J. Nanotechnol. 8 (2017) 2264–2270, https://doi.org/10.3762/bjnano.8.226.

[6] M. Li, S. Zhang, L. Li, J. Han, X. Zhu, et al., ACS Sustain. Chem. Eng. 8 (2020) 11465–11476, https://doi.org/10.1021/acssuschemeng.0c04829.

[7] L. Zhang, L. Zhang, Y. Chen, Y. Zheng, J. Guo, et al., ACS Sustain. Chem. Eng. 8 (2020) 5270–5277, https://doi.org/10.1021/acssuschemeng.0c00190.

[8] S. Zhang, X. Yin, Y. Zheng, Chem. Phys. Lett. 693 (2018) 170–175, https://doi.org/10.1016/j.cplett.2018.01.018.

[9] P. Raizada, V. Soni, A. Kumar, P. Singh, A.A. Parwaz Khan, et al., J. Mater. 7 (2021) 388–418, https://doi.org/10.1016/j.jmat.2020.10.009.

[10] A. Alhebshi, E. Sharaf Aldeen, R.S. Mim, B. Tahir, M. Tahir, Int. J. Energy Res. 46 (2022) 5523–5584, https://doi.org/10.1002/er.7563.

[11] Q. Guo, Q. Zhang, H. Wang, Z. Zhao, Catal. Commun. 103 (2018) 24–28, https://doi.org/10.1016/J.CATCOM.2017.09.010.

[12] P. Li, S. Zhu, H. Hu, L. Guo, T. He, Catal. Today 335 (2019) 300–305, https://doi.org/10.1016/J.CATTOD.2018.11. 068.

[13] C. Xin, M. Hu, K. Wang, X. Wang, Langmuir 33 (2017) 6667–6676, https://doi.org/10.1021/acs.langmuir.7b00620.

[14] R. Pang, K. Teramura, H. Asakura, S. Hosokawa, T. Tanaka, ACS Appl. Energy Mater. 2 (2019) 5397–5405, https://doi.org/10.1021/acsaem.9b00093.

[15] E. Kusiak-Nejman, J. Wojnarowicz, A.W. Morawski, U. Narkiewicz, K. Sobczak, et al., Appl. Surf. Sci. 541 (2021) 148416, https://doi.org/10.1016/j.apsusc.2020.148416.

[16] A.W. Morawski, K. Ćmielewska, E. Kusiak-Nejman, P. Staciwa, J. Kapica-Kozar, et al., J. CO_2 Util. 75 (2023) 102553. ⟨https://10.1016/j.jcou.2023.102553⟩.

[17] G. Nagaraju, Udayabhanu, Shivaraj, S.A. Prashanth, M. Shastri, et al., Mater. Res. Bull. 94 (2017) 54–63, https://doi.org/10.1016/j.materresbull.2017.05.043.

[18] R. Hachani, M. Lowdell, M. Birchall, A. Hervault, D. Mertz, et al., J. Nanoscale 8 (2016) 3278–3287, https://doi.org/10.1039/C5NR03867G.

[19] M.G. Kotresh, M.K. Patil, S.R. Inamdar, Optik 243 (2021) 167506, https://doi.org/10.1016/j.ijleo.2021.167506.

[20] D.D. Thongam, J. Gupta, N.K. Sahu, SN Appl. Sci. 1 (2019) 1030, https://doi.org/10.1007/s42452-019-1058-3.

[21] A. Kajbafvala, S. Zanganeh, E. Kajbafvala, H.R. Zargar, M.R. Bayati, et al., J. Alloy. Compd. 497 (1–2) (2010) 325–329, https://doi.org/10.1016/j.jallcom.2010.03.057.

[22] Z. Lin, F. Guo, C. Wang, X. Wang, K. Wang, et al., RSC Adv. 4 (10) (2014) 5122, https://doi.org/10.1039/c3ra45254a.

[23] J. Sithole, B.D. Ngom, S. Khamlich, E. Manikanadan, N. Manyala, et al., Appl. Surf. Sci. 258 (20) (2020) 7839–7843, https://doi.org/10.1016/j.apsusc.2012.04.073.

[24] J. Winiarski, W. Tylus, K. Winiarska, I. Szczygieł, B. Szczygieł, J. Spectrosc. 2018 (2018) 2079278, https://doi.org/10.1155/2018/2079278.

[25] L.Y. Lin, C. Liu, T.T. Hsieh, J. Catal. 391 (2020) 298–311, https://doi.org/10.1016/j.jcat.2020.08.036.

[26] K. Saruhashi, Pap. Meteorol. Geophys. 6 (1955) 38–55, https://doi.org/10.2467/mripapers1950.6.1_38.

[27] Y.-C. Huang, A. Rao, S.-J. Huang, C.-Y. Chang, M. Drechsler, et al., Angew. Chem. Int. Ed. 60 (2021) 16707–16713, https://doi.org/10.1002/ange.202104002.

[28] L. Wang, H. Tan, L. Zhang, B. Cheng, J. Yu, Chem. Eng. J. 411 (2021) 128501, https://doi.org/10.1016/J.CEJ.2021.128501.

[29] S. Yamabi, H. Imai, J. Mater. Chem. 12 (2002) 3773–3778, https://doi.org/10.1039/b205384e.

[30] M. Tasbihi, K. Kočí, I. Troppová, M. Edelmannová, M. Reli, et al., Environ. Sci. Pollut. Res. 25 (2018) 34903–34911, https://doi.org/10.1007/s11356-017-0944-8.